

Phosphine-stabilized hidden ground states in gold clusters investigated via a $Au_n(PH_3)_m$ database

Caitlin A. McCandler^{1,2}, Jakob C. Dahl^{2,3,4}, Kristin A. Persson^{1,4,*}

¹Department of Materials Science, University of California Berkeley, CA 94720, USA

²Materials Science Division, Lawrence Berkeley National Laboratory, Berkeley, CA 94720, USA

³Department of Chemistry, University of California Berkeley, CA 94720, USA

⁴Molecular Foundry, Lawrence Berkeley National Laboratory, Berkeley, CA 94720, USA

*Corresponding author: Kristin Persson, kapersson@lbl.gov

July 21, 2022

1 Abstract

Nanoclusters are promising materials for catalysis and sensing owing to their large surface areas and unique electronic structures which can be tailored through composition, geometry, and chemistry. However, relationships correlating synthesis parameters directly to outcomes are limited. While previous computational studies have mapped the potential energy surface of specific systems of bare nanoclusters by generating and calculating the energies of reasonable structures, it is known that environmental ions and ligands crucially impact the final shape and size. In this work, phosphine-stabilized gold is considered as a test system and DFT calculations are performed for clusters with and without ligands, producing a database containing >10,000 structures for $Au_n(PH_3)_m$, ($n \leq 12$). We find that the ligation of phosphines affects the thermodynamic stability, bonding, and electronic structure of Au nanoclusters, specifically such that ‘hidden’ ground state cluster geometries are stabilized that are dynamically unstable in the pure gold system. Further, the addition of phosphine introduces steric effects that induce a transition from planar to non-planar structures at 4-5 Au atoms rather than up to 13-14 Au atoms as previously predicted for bare clusters. This work highlights the importance of considering the ligand environment in the prediction of nanocluster morphology and functionality, which adds complexity as well as a rich opportunity for tunability.

2 keywords

nanoclusters, gold, phosphine, ligands, DFT, high-throughput, synthesis

3 Introduction

Nanoclusters (NCs), a class of ultra-small nanoparticles, are promising materials for catalysis, fluorescent sensors, bioimaging, nanomedicine and precursors for nanoparticle synthesis. These materials measure less than 1 nm (<150 atoms) and exhibit molecular-like electronic structures as well as irregular atomic configurations. Their electronic and physico-chemical properties are highly dependent on their composition, size, atomic configuration, and surface functionalization. Additionally, NCs exhibit large surface areas that are ideal for catalyzing reactions and discrete electronic states for optical applications.

Over the past two decades, nanoclusters have been synthesized with increasing diversity and identified with atomic-level precision. This has led to greater interest in *directing* the synthesis to design specific new shapes and sizes. However, experimental nanocluster synthesis is time-intensive due to the difficulty of isolating nanoclusters in high enough purity for X-ray crystallography. Synthetic yields can be low due to poor selectivity, and transient, metastable intermediate clusters may be difficult to isolate or probe with in-situ characterization.

Hence, improved predictions of stable structures, intermediate clusters and possible reaction pathways provide a guide to possible synthesis products of specific structure and size, as well as fundamental understanding of how these nanoclusters form.

Solution-based growth is the preferred method to synthesize nanoclusters for several reasons. Firstly, it offers the introduction of protective ligands to improve separation, storage and size control¹. Secondly, solvated nanoclusters are required for solution-based processes including photocatalysis, thin film processing and drug delivery. Combinations of ligands can provide a variety of stable configurations and surfaces, and result in highly variable performance. Importantly, ligation has been shown to be more effective at controlling the synthesis product than using kinetic control². It is clear that cluster thermodynamic stability as well as electronic structure and bonding are fundamentally influenced by the presence of ligands.

The structural and thermodynamic landscape of nanoclusters can be effectively explored using computational techniques. Indeed, global structure searching studies have extensively characterized the potential energy surface (PES) for bare gold clusters in the gas phase and have been highly successful in predicting the products of gold vaporization³⁻¹⁹. Additional work has been done to predict the geometry of the ligand shell given the precise locations of the metal core atoms²⁰, to monitor the impact of SCH_3 on Au_{11} ²¹, PH_3 on Au_{13} ²² and Au_8 ²³, PH_3 and Cl on Au_{55} ²⁴, and $PH_2(CH_2)_M PH_2$ (spacer M = 3, 5) on cationic Au_n (n = 7-11)²⁵. However, to the best of our knowledge, there has been no work examining how ligation changes the sequence of stable cluster geometries,

effectively stabilizing otherwise ‘hidden’ ground states.

Here we present an extensive, grand canonical, data-driven study on ligated gold clusters, spanning >10,000 unique structures. We map the impact of ligation on the core gold structure (gold kernel), and analyze trends in preferred ligand binding sites, ground state geometries, and hybridizations of gold-gold bonding. As a model ligand, we select phosphine, which exhibits weaker binding energies than thiolate ligands, and is hence more suitable for catalysis²⁶ and leads to less structural rearrangement. We show that, for the open system of phosphine and gold, phosphine ligation constitutes a crucial factor in the global search for stable nanocluster ground states.

4 Results and discussion

4.1 Population Distribution

The ligation generation algorithm (see Computational Methods and Details) resulted in 10,868 unique $Au_n(PH_3)_m$ ($n \leq 12$) structures, which includes the initial set of pure gold structures, as well as an addition of the monomer, dimer, and experimental structures from the CSD²⁷. Due to the relaxation of a gold core in presence of ligands, a highly diverse set of nanoclusters were produced. In total we obtained 4516 new unique geometries, as defined by having different gold structures to the original set. Details of the energy distribution and the number of structures calculated for each size are shown in Figure ???. Larger gold core sizes generated more structures due to the increased combinatorial space of ligand sites. It should also be noted that the initial gold kernels were the lowest energy species in the previously performed global energy search conducted to create the Quantum Cluster Database¹⁷, and as such are useful for the comparison with the PES of bare gold NCs.

The weaker binding energy and the single lone pair of electrons in phosphine ligands leads to a simple radial monodentate binding motif, which is easier to model than the complicated ‘staple’ motif that thiolate ligands with three lone pairs available for binding adopt. Also, the weaker binding of phosphine causes less structural rearrangement of the gold NC core. Finally, a simple PH_3 ligand can be substituted for the more complex but more commonly used triphenyl phosphine (PPh_3) to reduce the computational cost while still capturing some of the steric interactions, unlike halides. However, we emphasize that some important differences to experimentally used ligands remain, including less steric hindrance, weaker binding energies, less electronegativity, and less polarizability²⁸⁻³¹.

4.2 Grand Canonical Energy Formulation

The grand canonical energies of the structures were obtained according to

$$E_{GC} = E - n\mu_{Au} - m\mu_{PH_3} \quad (1)$$

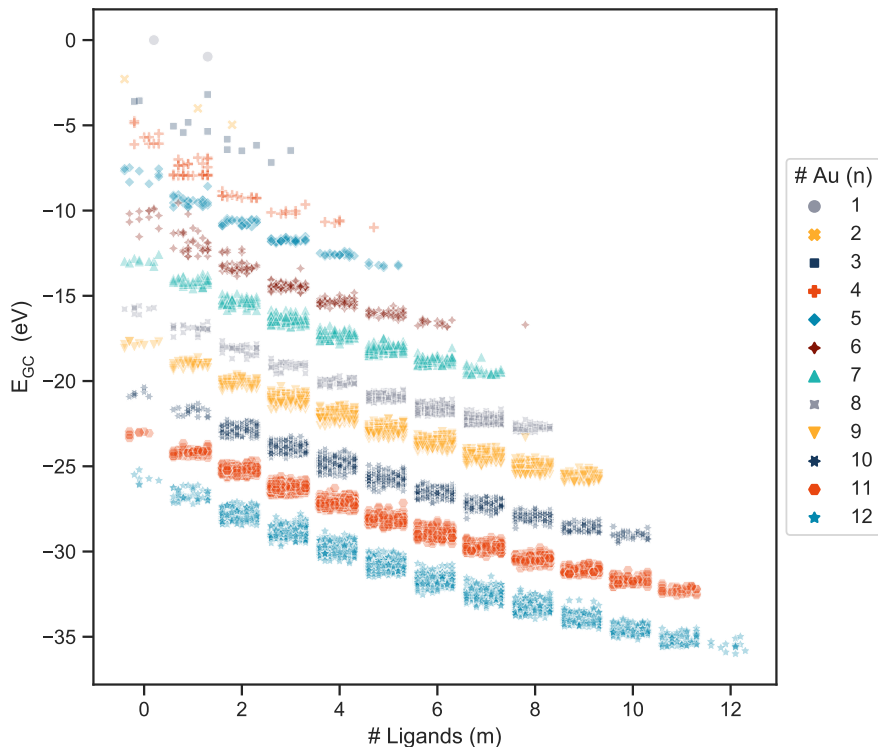


Figure 1: Grand canonical energies of the >10,000 structures in the dataset, including the experimental set. $\mu_{Au} = -0.29$ eV and $\mu_{PH_3} = -15.62$ eV.

where n represents the size of the gold cluster (number of gold atoms), and m represents the number of PH_3 ligands in the cluster. All subsequent discussion of energy will refer to the grand canonical energy.

The chemical potentials of gold and phosphine, μ_{Au} and μ_{PH_3} , were calculated with DFT as the total energy of a gold atom and a phosphine complex in vacuum and were obtained as -0.29 eV and -15.62 eV respectively. The grand canonical energies of all structures in the dataset are shown in Fig. 1, as a function of the number of bonded ligands.

We note that there is likely a window of relevant chemical potentials, accessible by tuning the composition and concentration of the solution. For example, by applying the entropy correction of phosphine in the gas phase at 300K provided in the NIST database³², the resulting chemical potential of phosphine would lower to -16.28 eV/ PH_3 . Lower chemical potentials indicate a more stable environmental phosphine state, which competes strongly with the gold nanocluster ligation. We find that using the NIST gas phase value results in sparingly ligated ground states, in contrast with experimental observations. Hence we ex-

pect that most relevant solution chemical potentials of phosphine to be higher than -16.28 eV. Using the higher DFT calculated μ_{PH_3} , we find that ligand binding energy tapers off when sizes, n , are equal to number of ligands, m . The ligand binding energy also decreases for larger structures of gold, meaning that a ligand is more stabilizing for smaller structures. The most stable structures of all ground states with $n = m$ were examined for ligand saturation, however none of the structures, given the starting positions, were able to accommodate another ligand. Some experimentally realized structures, however, are able to bind more ligand head groups than gold atoms, typically by utilizing bidentate ligands (CSD IDs: 1541477³³, 1009716³⁴, 862706³⁵).

4.3 Thermodynamic Stability Ranking

We find that the predicted ground states, and thermodynamically ranked isomers depend strongly on the number of ligands bound to the nanocluster. This demonstrates that ligands stabilize some geometries more than others, and that using the bare nanocluster energy rankings is not sufficient to predict the sequence of stable nanocluster structures as a function of size in an environment where ligating species are available.

In order to analyze the impact of ligands on the relative thermodynamic stability, structures with the lowest energy for a given gold kernel geometry were identified from each set of structures with n gold atoms and m ligands. Figure 2 shows the differences in the thermodynamic stability between the isomers and the ground state structure with the same number of m ligands for a representative 7 gold atom kernel size. All other sizes between $n=3-12$ are included in Fig. ???. Relevant gold kernel geometries are identified and show large differences in calculated energies above the hull as a function of ligation. Importantly, we find that structures that have been observed experimentally (CSD IDs: 2023935³⁶, 668368³⁷, 1123093³⁸, 1123094³⁹, 1123095⁴⁰) were correctly identified as ground states only with $m=6$ and $m=7$. Notably, these structures are 200 meV and 470 meV above the hull, respectively, in their bare, unligated state. Further, the ground state bare Au_7 cluster is not present in the $Au_7(PH_3)_7$ set because the core gold geometry undergoes significant reorganization to accommodate 7 ligands; hence there is no structure-matched equivalent ligated structure.

Below, we summarize some of the findings and comparisons to experimental synthesis products for each gold kernel size, n . In these comparisons, it is important to keep in mind that synthesis procedures involve crystallization and other post-synthesis techniques in order to improve selectivity. Also, any experimental structure that relaxed away from the geometry (and bonding) reported in the CSD were not considered as experimental references but are included in the dataset.

n=4: The experimentally realized Au_4 structure is a tetrahedron with 4 ligands (CSD IDs: 1206655⁴¹, 1231463⁴²). The bare tetrahedral structure is energetically unfavorable in computations, though it becomes notably more stable with ligation, improving agreement with experimental observations.

n=6: Two experimental clusters are considered (CSD IDs: 1120743⁴³,

1272194⁴⁴). These structures are slightly distorted from a square bipyramidal geometry and an octahedral geometry, and were ranked 5th and 9th among the computed $Au_6(PH_3)_m$, at 14 meV/Au and 55 meV/Au above the most stable cluster. The two most theoretically stable gold kernels differ from the lowest energy experimental structure only by the rearrangement of 1 gold atom. Without ligation, the most stable Au_6 structure is a planar triangle, but with ligation this planar structure is destabilized to 29 meV/Au above the most stable n=6 structure.

n=8: Two experimental structures retained their initial geometry during DFT relaxation and are considered here: one with $m=7$ and a hexagonal base structure (CSD IDs: 1106337⁴⁵, 1106336⁴⁶) and one with $m=8$ and an extended structure with a rhombus base motif (CSD ID: 1001047⁴⁷). The computed energies of these clusters were relatively high and ranked 55th (72 meV/Au) and 40th (58 meV/Au) respectively within the $Au_8(PH_3)_m$ structures. A lower chemical potential of phosphine, μ_{PH_3} , would lower the relative energy of the $Au_8(PH_3)_7$ experimental structure as it is not fully saturated with ligands. The $Au_8(PH_3)_8$ experimental structure is likely high in energy with monodentate PH_3 ligands as it was synthesized with bidentate ligands. The Au_8 kernel that is the most stable in the bare system by 41 meV/Au can only accept 4 ligands before it breaks its 4-fold (square) symmetry or becomes highly energetically unfavorable.

n=9: Four unique experimental $Au_9(PH_3)_8$ structures were used as references, each having one central unligated Au atom. They are ranked 33rd (43 meV/Au) with octahedral geometry (CSD ID: 1967410⁴⁸), 51st (57 meV/Au) with 'butterfly' geometry (CSD IDs: 615444⁴⁹, 687192⁵⁰, 1273985⁵¹), 52nd (57 meV/Au) with 'crown' geometry (CSD IDs: 690419⁵², 690422⁵³, 615445⁵⁴, 690418⁵⁵), and 84th (81 meV/Au) with 'distorted crown' geometry (CSD IDs: 1895800⁵⁶, 1895797⁵⁷) above the $Au_9(PH_3)_m$ hull, respectively. The 'distorted crown' experimental structure is likely high in energy with monodentate PH_3 ligands as it was synthesized with bidentate ligands.

4.4 Hidden Ground States

Many of the ligated structures exhibit gold kernels that are not local energy minima in the PES without ligation (i.e. there is no energy barrier between the geometry and a lower energy geometry). These structures are truly *hidden ground states*⁵⁸ such that they are dynamically unstable (e.g. a saddle point in the PES) in a pure gold system. An example of a hidden ground state identified here is the $Au_8(PH_3)_8$ structure. In the case of this cluster, ligands stabilize a more 3D structure, labelled in Fig. 3 as (a), which is *dynamically* unstable in its bare form and relaxes to a markedly different structure, labelled (b). Hence, the $Au_8(PH_3)_8$ ground state structure cannot be obtained by naive ligation of the bare ground state. Similarly, the ground state $Au_5(PH_3)_5$ manifests a 3D structure, but spontaneously relaxes into a 2D geometry when the ligands are removed. The presence of such hidden ground states is an indication that a gold cluster PES is significantly affected by ligation. Hence, a pool of unli-

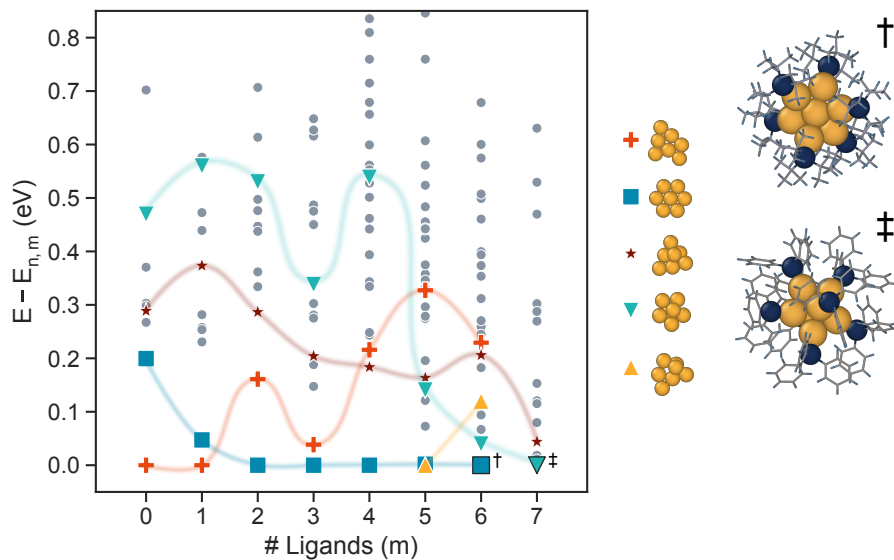


Figure 2: Energies of $Au_7(PH_3)_m$ isomers for varying number of ligands, m , showing the strong influence of ligation. The energies are referenced to the minimum value for each m , $E_{7,m}$. Each point represents a unique gold kernel with the optimal ligand configuration for the given m ; four gold kernels are highlighted in order to demonstrate how relative energies change with ligation. Experimental structures from literature sourced from the CSD are denoted with black outlines. Here, experimental structures are the lowest in the energy orderings for 6^\dagger (CSD ID: 2023935³⁶) and 7^\ddagger (CSD IDs: 668368³⁷, 1123094³⁹, 1123093³⁸, 1123095⁴⁰) ligands.

gated metastable structures is likely to miss potential synthesis products and neglecting the effect of ligation leads not only to a shift in the relative energies of different geometries but also to overlooking specific ground states entirely.

To explore the prevalence of hidden ground states, we examined the ground state structures - for all combinations of n atoms and m ligands - for metastability in their unligated state. From this analysis, 25 structures out of the 75 total ground states ($3 \leq n \leq 12$, $1 \leq m \leq n$) and 6 out of the 10 fully ligated structures ($n = m$) were found to be hidden ground states. The full list of ground state structures is included in ST1.

4.5 Planar to Non-planar Transition

The size dependence of the planar to non-planar transition of gold clusters is relevant for predicting structure-function correlations. However, most of the work has focused on bare clusters in the gas phase⁴⁻¹⁸ and predicts large planar

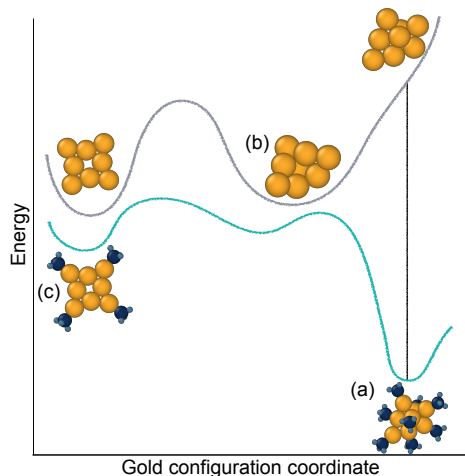


Figure 3: An illustration of the concept of hidden ground states, where the energy for bare gold and ligated gold are sketched as a function of a schematic gold configuration coordinate. Structure (a) is a hidden ground state as it is the most stable $Au_8(PH_3)_8$ structure in the dataset, but relaxes to structure (b) when its ligands are removed. Structure (c) is the most stable structure that can be achieved for the hollow square Au_8 kernel that is the most stable in the bare PES²³

to non-planar transition sizes, up to 13-14 Au atoms^{16,17}. Here we find that the 2D to 3D transition in ligated systems occurs much earlier, with the transition occurring between 4 to 5 gold atoms. This finding better represents the early transition size of 3 to 4 gold atoms observed experimentally. Tetrahedral Au_4 structures have been synthesized and characterized experimentally with bulky ligands: $[Au_4(P(mesityl)_3)_4]^{2+41}$ and $[Au_4(P(tert-Bu)_3)_4]^{2+42}$. We speculate that if more bulky ligands were used in this study, like PPh_3 , the size at which the transition occurs could be lowered further and recreate the experimental 2D to 3D transition size of 3 to 4 gold atoms. Fig. 4 quantifies the degree to which the relative energy between 2D and 3D structures changes with the addition of ligands. Structures are defined to be planar (2D) if the average squared distance of gold atom positions to an optimal fitting plane is less than 0.1 Å. Positive values indicate that a 2D structure is preferred and negative values indicate that a 3D structure is preferred.

We find 3D structures to be preferable for ligated structures for two main reasons: sterics and s-d hybridization. Both effects will be discussed in the following sections.

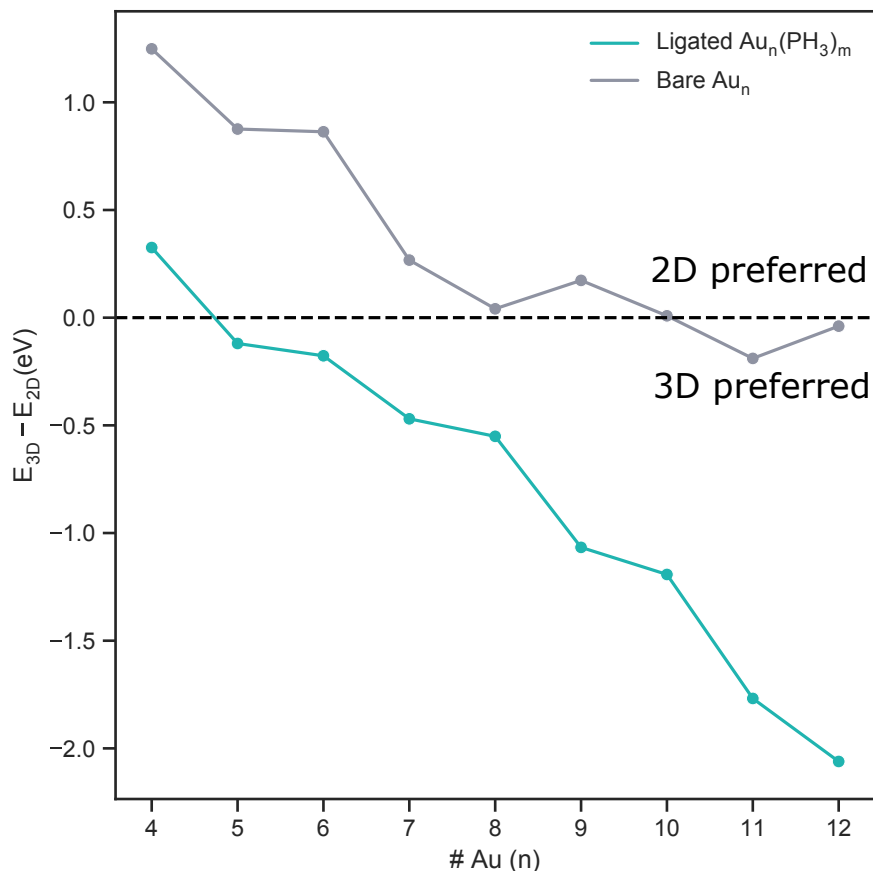


Figure 4: The energy difference ($\Delta E = E_{3D} - E_{2D}$) between the most stable 2D and 3D clusters as a function of cluster size, as predicted with and without ligation.

4.6 s-d Hybridization

Bare gold nanoclusters have been extensively investigated for the role of s-d hybridization in stabilizing planar configurations; While many argue that hybridization between the 5d and 6s orbitals is the key factor in stabilizing the planar gold structures^{59,60}, others have found that effects such as vdW interactions¹⁴ and d-electron delocalization⁶¹ are more important. Shafai et. al. noted a shift in the d-band center in $Au_{13}(PH_3)_{12}$ to lower energies for more 3D geometries, as well as increased Au s-d overlap with the P p-orbitals in 3D structures, while planar structures exhibit both bonding and anti-bonding contributions²². Spivey et. al. found that 3D geometries allow for better orbital mixing in $Au_{11}(SCH_3)_m$ of S p-orbitals and Au d-orbitals²¹.

Here we find a strong correlation between higher s-d hybridization and 2D configurations of gold, as suggested by literature, and exemplified in Fig. ?? for a representative cluster size of $n = 12$. We further examine how the s-d hybridization is affected by ligation. Figure 5 shows the trend in stabilization from s-d hybridization, H_{sd} (as calculated per Eq. 3 in Section 5.2), as a function of ligation. As shown, there is a distinct increase in energy (destabilization) with respect to s-d hybridization, H_{sd} , as a function of ligation. Given that phosphine exhibits a weaker binding energy as compared to other widely-used ligands such as thiolates, these effects will likely be even more pronounced in systems with stronger binding energies.

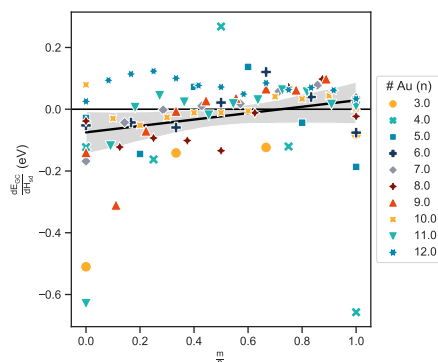


Figure 5: The derivative of grand canonical energies with respect to s-d hybridization index, $\frac{dE_{GG}}{dH_{sd}}$, for each set of cluster sizes, n and m . The positive trend line indicates that clusters are destabilized with greater s-d hybridization at higher ligand coverage (ratio of ligands to gold atoms, $\frac{m}{n}$). Note that clusters with n atoms and m ligands with 4 or fewer datapoints were not considered due to poor statistics. S-d hybridization is responsible for the stabilization of 2D structures in the bare gold system. 3D structures are more stable when ligated, possibly having to do with this trend in reduced stabilization from s-d hybridization with more ligands.

4.7 Steric Effects

To analyze the local environment of the ligand binding sites and its impact on the cluster energy, we calculate the distances between neighboring ligands and evaluate the gold binding site topology. Analyzing the trends we observe two similar but distinct steric effects. First, the steric repulsion of ligands in close proximity favors structures where the ligands maximize their distance from each other. Extrapolating to bulkier ligands, such as PPh_3 , it is likely that these effects will be amplified due to the larger radius of steric interaction. Secondly, we find that corner sites are preferred over edges and faces (see Fig. ??). Comparing mono-ligated structures (i.e. $Au_n(PH_3)_1$), we classify the

structures by ligand binding site (corner, or edge/face) by examining all bond angles between the binding gold atom and its neighboring gold atoms. Corner bonds are then defined as having Au-Au-Au (central Au is the binding Au) bond angles no greater than 140° . All structures with the same gold geometry were then compared according to their classifications. Indeed, corner-bound ligands were found to exhibit an average of 361 meV stronger binding energy than ligands bound to edges and faces of gold. Importantly, for larger sizes with saturated ligation, this preference for corners over edges lead initially planar structures to relax into 3D structures during geometry optimization in order to create more corner and edge sites.

4.8 $Au_n(PH_3)_m$ Phase Diagram

To explore the phase space of most stable PH_3 -ligated Au clusters, we compute the grand canonical energy (Eq. 1) for a range of chemical potentials, μ_{Au} and μ_{PH_3} , reflecting the ability to control these parameters through the concentration of precursors in solution. Additionally, the ligand binding energy, $E_{binding}$, related to chemical potential according to Eq. 2 below, also correlates to the sterics and electron donating properties of the ligand and can thus be changed by utilizing different chemical species⁶².

$$E_{binding} = -\mu_{PH_3} + (E_{n,m+1} - E_{n,m}) \quad (2)$$

To estimate a synthesis yield based on relative energies, we assume that the structure population follows a Boltzmann distribution at 300K. The results are shown in Fig. 6, which prompts us to make the following observations. Changes between which structures are the most stable in the grand canonical ensemble only occur at very low chemical potentials of gold. The gold monomer and dimer occupy a large portion of the available phase space. However, at higher gold chemical potential, we find favorable conditions for small cluster formation, with a range of ligation as a function of phosphine chemical potential. At high phosphine chemical potential there is a strong stabilization of the largest, fully ligated cluster (here $Au_{12}(PH_3)_{12}$), indicative of crystallization. We note that $n=12$ is the limit of this dataset, and it is likely that larger sized clusters would successfully compete at these conditions.

A number of factors can influence the agreement between Fig. 6 and experimental outcomes, and we emphasize that our findings should be taken as trends within chemical potential space, rather than pinpointing absolute values. For example, careful benchmarking work has shown DFT to exhibit errors in estimating the Au_2 binding energy³¹. An equivalent construction of a phase diagram included in Fig. ?? shows the structures that might exist aside from the monomers and dimers.

4.9 Proposed Nanocluster Growth Mechanism

During a solution synthesis reaction of gold NCs, gold is reduced from Au (I) or Au (III) precursors. Hence, the concentration and thus the chemical poten-

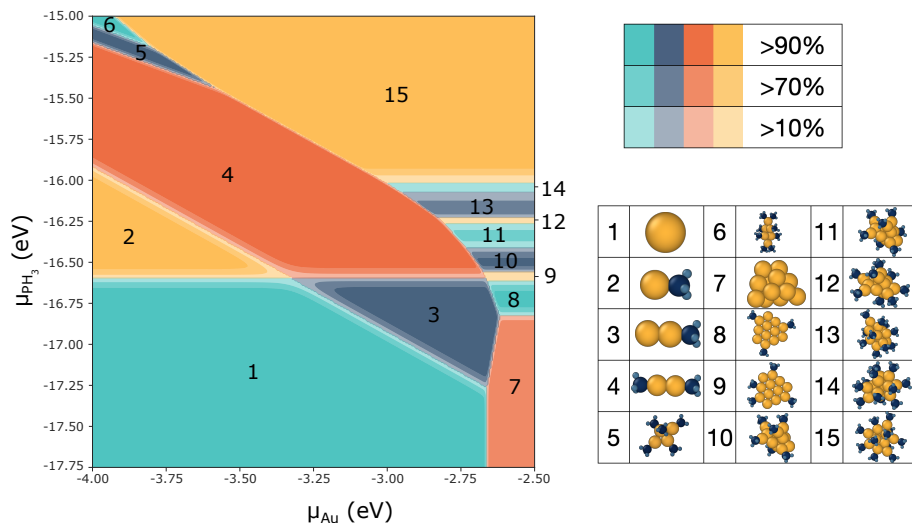


Figure 6: The $Au_n(PH_3)_m$ phase diagram was created by finding the most stable structure in the dataset for a range of chemical potentials. The stable species are shown on the right. The fraction of the solution product that they would expect to represent is calculated at 300K via Boltzmann population statistics.

tial of Au (0) are expected to monotonically increase, providing a measure of relative reaction progress. As a result, the sequence of lowest energy structures as a function of Au chemical potential corresponds to a set of metastable intermediates in a growth mechanism if rearrangement of the internal structure is fast. At transition points, i.e. chemical potentials at which the grand canonical energies of two stable intermediates Au_{n1} and Au_{n2} are equal, the lowest energy structures of gold clusters Au_{nx} ($n1 < nx < n2$) then present unstable intermediates, or transition state structures. We can propose a nanocluster growth mechanism based on the lowest energy structures as a function of gold chemical potential. An example sequence of potential metastable intermediate clusters for a phosphine chemical potential of -15.9 eV is included in Fig. 7. We note that one of the intermediates in this reaction pathway (size 7) has been successfully synthesized (CSD IDs: 668368³⁷, 1123094³⁹, 1123093³⁸, 1123095⁴⁰).

While including ligation significantly improves the qualitative agreement between observed and predicted clusters, there are a few remaining questions and discrepancies. For example, calculated intermediates with odd numbers of gold atoms are systematically predicted to be higher in energy than the even-sized structures. Different odd-even behavior has been computationally reported and we observe the same trend here (see Fig. ??) with even-sized structures being predicted to be more stable than odd-sized structures^{5,7,63-65}, however this behavior is not supported by experimental evidence. We do, however, note that even- and odd-sized clusters synthesized experimentally all exhibit even and odd cationic charges, respectively. Thus, using a neutral (even) charge may

preferentially favor even-sized clusters.

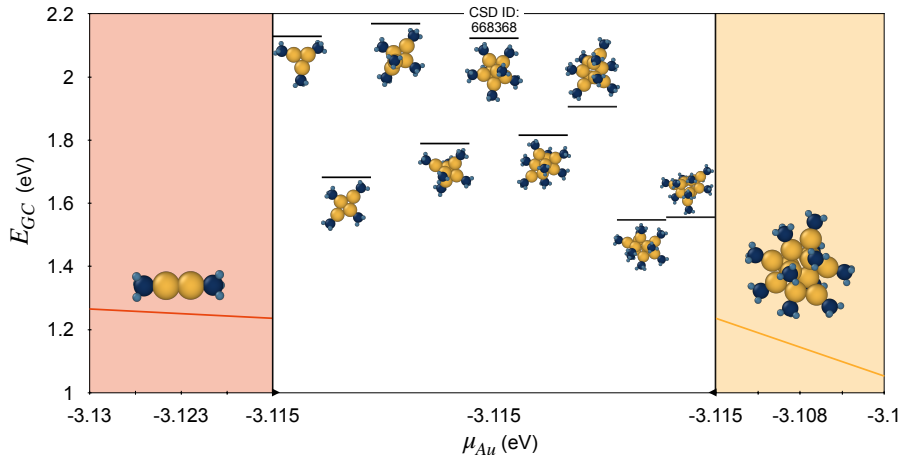


Figure 7: Proposed reaction mechanism. The idealized reaction that would have to occur to transition from one ground state to another with increasing μ_{Au} and constant $\mu_{PH_3} = -15.9$ eV. One of these intermediates has been previously synthesized and reported (CSD IDs: 668368³⁷, 1123094³⁹, 1123093³⁸, 1123095⁴⁰)

5 Methods

5.1 Ligation Algorithm

A database of phosphine-ligated nanoclusters is generated from an initial set of bare structures as outlined below and illustrated in Fig. 8. The algorithm is divided into steps i)-v) as follows (the same numbers are used in Fig. 8).

i) **Initial structures.** A group of previously predicted low energy bare gold clusters is defined from the Quantum Cluster Database¹⁷. 81 structures between 3 to 12 atoms with low energies are taken as the initial set of gold cluster geometries.

ii) **Addition of ligands.** A new structure with an additional PH_3 ligand is created for each possible ligand binding site. Binding sites are identified as gold atoms on the surfaces of the clusters that do not already have a bond to a PH_3 ligand. Reasonable guesses for optimal ligand placements are made with a Fruchterman-Reingold force-directed algorithm, implemented by the *networkx* code, which treats the new bond between the Au and P as a spring and then adds electrostatic repulsion so that the new ligand is positioned away from the cluster.

iii) **Pruning.** Each structure is compared to all others in the set and any duplicate or symmetrically equivalent structures are removed. Structures are defined as duplicates if they have isomorphic bonding (Au-Au and Au-P bond

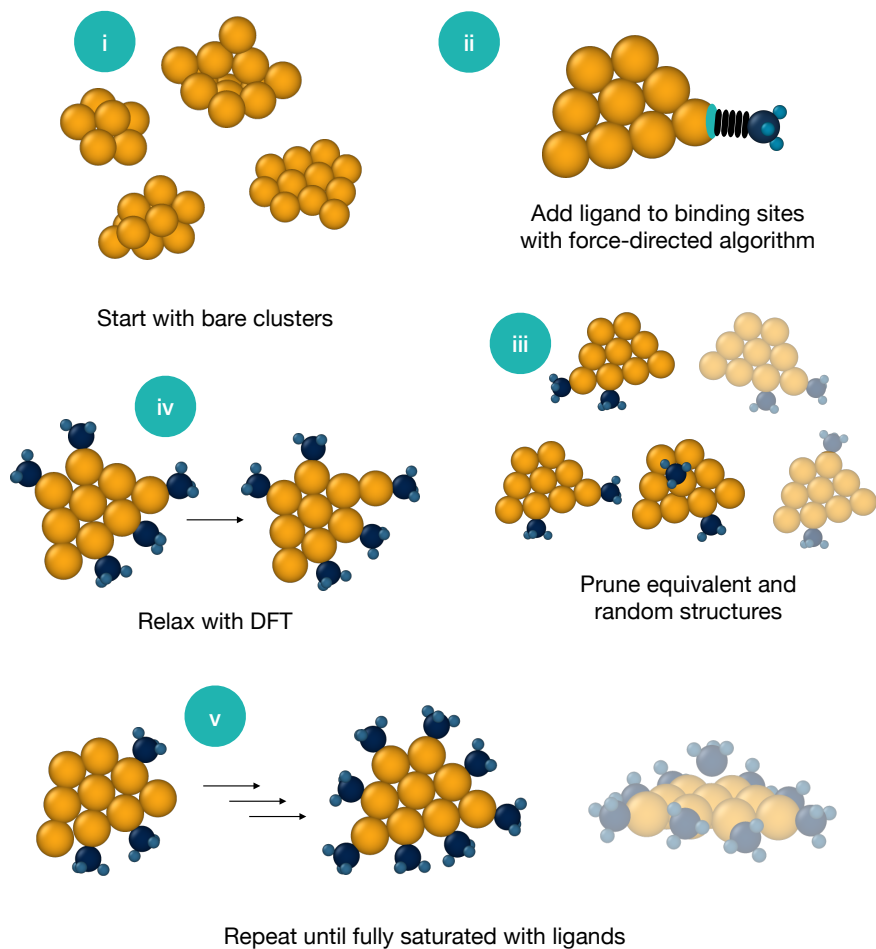


Figure 8: Ligation Algorithm. New ligated clusters were generated by adding PH_3 successively onto bare gold clusters.

cutoffs of 3.2 and 2.5 Å, respectively). In order to manage the combinatorial explosion of possible partially-ligated structures, a random fraction of structures with duplicate gold kernels were removed under the assumption that those remaining constituted a sufficient sampling of possible partially-ligated structures. The fraction of pruned structures correlated with the structure size and number of combinations of ligand configurations; As many as 90% of the largest structures ($n=12$) with half ligation ($m=6$) were pruned, while none of the smaller ($n < 8$) or fully ligated ($n=m$) structures were pruned.

iv) **Relaxation.** The structures are geometrically relaxed with DFT.

v) **Repeat and terminate.** Steps ii)-iv) are repeated until the structures are fully saturated with ligands. Over-saturation is achieved when the last ligand does not bind to the cluster (Au-P distance $>2.5\text{\AA}$), and such structures are excluded in the final set. At this point, the algorithm terminates. We note that the outlined sequential procedure - which adds one ligand at a time and relaxes that cluster - does not target highly symmetric ligated structures.

5.2 Computational Methods and Details

The structures of $Au_n(PH_3)_m$ are geometrically relaxed with density functional theory (DFT). Additionally, 50 phosphine-stabilized gold structures from the Cambridge Structural Database (CSD) were computed with PH_3 in place of their organophosphine (PR_3) ligands. 24 of those (12 unique structures) maintained the same structures and gold bonding (Au-Au bond cutoff of 3.2\AA) during DFT geometry optimization and were taken as a set of reference experimental structures.

Spin-polarized calculations were performed with a plane wave basis set, as implemented in the Vienna Ab-initio Simulation Package (VASP)⁶⁶. A cutoff energy of 520eV was applied for the plane wave basis set and the electron-ion interactions were described by the projector augmented wave (PAW) method⁶⁷. The exchange and correlation energies were calculated using the Perdew-Burke-Ernzerhof (PBE) form of the generalized gradient approximation (GGA)⁶⁸. The structures were provided at least 10\AA of vacuum along each direction to reduce self-interaction between periodic images^{69,70}. One k point, i.e., the γ point, was used in the cluster calculations and Gaussian smearing was applied with a width of 0.2 eV. Spin orbit coupling was not considered given its computational cost and contradicting conclusions regarding its effect on the relative stability of bare Au clusters^{3,7}. A post-relaxation dispersion energy correction with zero damping (D3) was then applied⁷¹.

The s-d hybridization, H_{sd} , is calculated according to the method described in literature and reproduced in Eq. 3^{14,72}, where variable I represents the atom index, S represents the spin state, W_E represents the occupation of the eigenvalue E, and m represents the index of d-orbitals. w_s and w_d are the weights of the projected wavefunction on the spherical harmonics within the Wigner-Seitz atomic radius around each atom;

$$H_{sd} = \sum_{I,S} \sum_E W_E^2 \sum_m w_s^{I,S,E} w_{d,m}^{I,S,E} \quad (3)$$

where only contributions from the orbitals of gold atoms were considered. An example graph of the DOS for a bare gold and ligated structure decomposed into s and d states is included in Fig. ??.

6 Conclusions and Future Work

We generate and calculate - by a first-principles grand-canonical formalism - thousands of $\text{Au}_n(\text{PH}_3)_m$ nanocluster structures to compare and analyze stability-promoting chemistry-structural trends. We find that the addition of phosphine ligands dramatically changes the bonding and hybridization in gold NCs such that the planar to non-planar transition occurs between $n=4$ and $n=5$, earlier than predicted for the bare gold system and in improved agreement with experimental observations. The stabilization of 3D cluster geometries in the presence of ligation is rationalized by a combination of steric effects and s-d hybridization analysis. Furthermore, ligation stabilizes cluster geometries that are dynamically unstable in a pure gold system, resulting in a significant population of ‘hidden ground states’. These new ground states manifest themselves in phase maps of cluster stability as a function of chemical potential, which lends insight into possible formation mechanisms. Our approach showcases the necessity of including ligands in calculations of nanocluster energies, as well as the predictive power of utilizing high-throughput DFT methods to map out potential gold nanocluster products and their formation pathways.

Simplifications employed here that are likely to further influence the stability of Au NCs include the use of PH_3 instead of bulkier PR_3 groups, the absence of solvation effects and the neutral charge states. We expect that the treatment of charge will reduce the odd/even energetic disparity and that the increased steric repulsion of bulkier ligands will promote more compact clusters. Future inclusion of these effects as well as increased cluster size is anticipated to guide practitioners to new experimental conditions and suggest formation mechanisms that can be empirically tested.

7 Data

The phosphine-stabilized gold structures are all publicly accessible on MPContribs at the following link <https://contribs.materialsproject.org/projects/auph3>

8 Acknowledgements

C.A.M. acknowledges useful discussions with John Dagdalen, Matthew Horton and Ryan Kingsbury. C.A.M., J.C.D., and K.A.P. thank the U.S. Department of Energy, Office of Science, Office of Basic Energy Sciences, Materials Sciences and Engineering Division, for their support under Contract No. DE-AC02-05-CH11231 within the Data Science for Data-Driven Synthesis Science grant (KCD2S2). This research used resources of the National Energy Research Scientific Computing Center, a DOE Office of Science User Facility supported by the Office of Science of the U.S. Department of Energy under Contract No. DE-AC02-05CH11231 using NERSC award BES-ERCAP0020531 and award BES-ERCAP0013481. C.A.M. gratefully acknowledges the National Defense Science and Engineering Graduate (NDSEG) fellowship for financial support.

J.C.D. acknowledges support by the National Science Foundation Graduate Research Fellowship under DGE 1752814 and by the Kavli NanoScience Institute, University of California, Berkeley through the Philomathia Graduate Student Fellowship.

References

- [1] Tsubasa Omoda, Shinjiro Takano, and Tatsuya Tsukuda. “Toward Controlling the Electronic Structures of Chemically Modified Superatoms of Gold and Silver”. In: *Small* 17.27 (2021), p. 2001439. ISSN: 1613-6829. DOI: 10.1002/smll.202001439.
- [2] John M. Pettibone and Jeffrey W. Hudgens. “Gold Cluster Formation with Phosphine Ligands: Etching as a Size-Selective Synthetic Pathway for Small Clusters?”. In: *ACS Nano* 5.4 (Apr. 2011), pp. 2989–3002. ISSN: 1936-0851, 1936-086X. DOI: 10.1021/nn200053b.
- [3] Maurício J. Piotrowski, Paulo Piquini, and Juarez L. F. Da Silva. “Density Functional Theory Investigation of 3 d , 4 d , and 5 d 13-Atom Metal Clusters”. In: *Phys. Rev. B* 81.15 (Apr. 2010), p. 155446. ISSN: 1098-0121, 1550-235X. DOI: 10.1103/PhysRevB.81.155446.
- [4] Himadri Sekhar De, Sailaja Krishnamurty, and Sourav Pal. “Understanding the Reactivity Properties of Au_n ($6 \leq n \leq 13$) Clusters Using Density Functional Theory Based Reactivity Descriptors”. In: *J. Phys. Chem. C* 114.14 (Apr. 2010), pp. 6690–6703. ISSN: 1932-7447. DOI: 10.1021/jp1004852.
- [5] Hannu Hakkinen and Uzi Landman. “Gold Clusters Au_n , $2 \leq n \leq 10$ and Their Anions”. In: (), p. 4.
- [6] Eva M. Fernández et al. “Trends in the Structure and Bonding of Noble Metal Clusters”. In: *Phys. Rev. B* 70.16 (Oct. 2004), p. 165403. ISSN: 1098-0121, 1550-235X. DOI: 10.1103/PhysRevB.70.165403.
- [7] Li Xiao and Lichang Wang. “From Planar to Three-Dimensional Structural Transition in Gold Clusters and the Spin–Orbit Coupling Effect”. In: *Chemical Physics Letters* 392.4 (July 2004), pp. 452–455. ISSN: 0009-2614. DOI: 10.1016/j.cplett.2004.05.095.
- [8] A. V. Walker. “Structure and Energetics of Small Gold Nanoclusters and Their Positive Ions”. In: *The Journal of Chemical Physics* 122.9 (Mar. 2005), p. 094310. ISSN: 0021-9606, 1089-7690. DOI: 10.1063/1.1857478.
- [9] Y. Dong and M. Springborg. “Global Structure Optimization Study on Au_{2-20} ”. In: *Eur. Phys. J. D* 43.1-3 (July 2007), pp. 15–18. ISSN: 1434-6060, 1434-6079. DOI: 10.1140/epjd/e2007-00059-y.
- [10] Behnam Assadollahzadeh and Peter Schwerdtfeger. “A Systematic Search for Minimum Structures of Small Gold Clusters Au_n ($N=2-20$) and Their Electronic Properties”. In: *J. Chem. Phys.* (), p. 12.

- [11] Wei Fa, Chuanfu Luo, and Jinming Dong. “Bulk Fragment and Tubelike Structures of Au N (N = 2 - 26)”. In: *Phys. Rev. B* 72.20 (Nov. 2005), p. 205428. ISSN: 1098-0121, 1550-235X. DOI: 10.1103/PhysRevB.72.205428.
- [12] Xi-Bo Li et al. “Size Dependence of the Structures and Energetic and Electronic Properties of Gold Clusters”. In: *The Journal of Chemical Physics* 126.8 (Feb. 2007), p. 084505. ISSN: 0021-9606, 1089-7690. DOI: 10.1063/1.2434779.
- [13] Mikael P. Johansson et al. “At What Size Do Neutral Gold Clusters Turn Three-Dimensional?” In: *J. Phys. Chem. C* 118.50 (Dec. 2014), pp. 29370–29377. ISSN: 1932-7447, 1932-7455. DOI: 10.1021/jp505776d.
- [14] Alper Kinaci et al. “Unraveling the Planar-Globular Transition in Gold Nanoclusters through Evolutionary Search”. In: *Sci Rep* 6.1 (Dec. 2016), p. 34974. ISSN: 2045-2322. DOI: 10.1038/srep34974.
- [15] Bryan R. Goldsmith et al. “Two-to-Three Dimensional Transition in Neutral Gold Clusters: The Crucial Role of van Der Waals Interactions and Temperature”. In: *Phys. Rev. Materials* 3.1 (Jan. 2019), p. 016002. ISSN: 2475-9953. DOI: 10.1103/PhysRevMaterials.3.016002.
- [16] Anderson S. Chaves, Maurício J. Piotrowski, and Juarez L. F. Da Silva. “Evolution of the Structural, Energetic, and Electronic Properties of the 3d, 4d, and 5d Transition-Metal Clusters (30 TM_n Systems for n = 2–15): A Density Functional Theory Investigation”. In: *Phys. Chem. Chem. Phys.* 19.23 (2017), pp. 15484–15502. ISSN: 1463-9076, 1463-9084. DOI: 10.1039/C7CP02240A.
- [17] Sukriti Manna et al. “A Database of Low-Energy Atomically Precise Nanoclusters”. In: (Dec. 2021). DOI: 10.26434/chemrxiv-2021-0fq3q.
- [18] Ping Wu, Qingxiu Liu, and Gang Chen. “Nonlocal Effects on the Structural Transition of Gold Clusters from Planar to Three-Dimensional Geometries”. In: *RSC Adv.* 9.36 (July 2019), pp. 20989–20999. ISSN: 2046-2069. DOI: 10.1039/C9RA02202C.
- [19] Stefan Gilb et al. “Structures of Small Gold Cluster Cations „Au_zn⁺, n=14. . . : Ion Mobility Measurements versus Density Functional Calculations”. In: *J. Chem. Phys.* 116.10 (2002), p. 8.
- [20] Sami Malola et al. “A Method for Structure Prediction of Metal-Ligand Interfaces of Hybrid Nanoparticles”. In: *Nat Commun* 10.1 (Sept. 2019), p. 3973. ISSN: 2041-1723. DOI: 10.1038/s41467-019-12031-w.
- [21] Kasi Spivey, Joseph I. Williams, and Lichang Wang. “Structures of Undecagold Clusters: Ligand Effect”. In: *Chemical Physics Letters* 432.1 (Dec. 2006), pp. 163–166. ISSN: 0009-2614. DOI: 10.1016/j.cplett.2006.10.012.
- [22] Ghazal Shafai et al. “Effect of Ligands on the Geometric and Electronic Structure of Au₁₃ Clusters”. In: *J. Phys. Chem. C* 113.28 (July 2009), pp. 12072–12078. ISSN: 1932-7447, 1932-7455. DOI: 10.1021/jp811200e.

- [23] Juan C. Burgos, Sol M. Mejía, and Gregory F. Metha. “Effect of Charge and Phosphine Ligands on the Electronic Structure of the Au₈ Cluster”. In: *ACS Omega* 4.5 (May 2019), pp. 9169–9180. ISSN: 2470-1343, 2470-1343. DOI: 10.1021/acsomega.9b00225.
- [24] Ganga Periyasamy and F. Remacle. “Ligand and Solvation Effects on the Electronic Properties of Au₅₅ Clusters: A Density Functional Theory Study”. In: *Nano Lett.* 9.8 (Aug. 2009), pp. 3007–3011. ISSN: 1530-6984. DOI: 10.1021/nl901430k.
- [25] Sampyo Hong et al. “Toward an Understanding of Ligand Selectivity in Nanocluster Synthesis”. In: *J. Phys. Chem. C* 115.30 (Aug. 2011), pp. 14478–14487. ISSN: 1932-7447. DOI: 10.1021/jp201723b.
- [26] Marshall R. Ligare, Grant E. Johnson, and Julia Laskin. “Observing the Real Time Formation of Phosphine-Ligated Gold Clusters by Electrospray Ionization Mass Spectrometry”. In: *Phys. Chem. Chem. Phys.* 19.26 (2017), pp. 17187–17198. ISSN: 1463-9076, 1463-9084. DOI: 10.1039/C7CP01402C.
- [27] C. R. Groom et al. “The Cambridge Structural Database”. In: *Acta Cryst B* 72.2 (Apr. 2016), pp. 171–179. ISSN: 2052-5206. DOI: 10.1107/S2052520616003954.
- [28] Sergei A. Ivanov, Indika Arachchige, and Christine M. Aikens. “Density Functional Analysis of Geometries and Electronic Structures of Gold-Phosphine Clusters. The Case of Au₄(PR₃)₄²⁺ and Au₄(μ₂-I)₂(PR₃)₄.” In: *J. Phys. Chem. A* 115.27 (July 2011), pp. 8017–8031. ISSN: 1089-5639, 1520-5215. DOI: 10.1021/jp200346c.
- [29] Y. Q. Qiu et al. “DFT/FF Study on Electronic Structure and Second-Order NLO Property of Dinuclear Gold Complex [Au(SeC₂B₁₀H₁₁)(PPh₃)₂].” In: *Synthetic Metals*. Proceedings of the International Conference on Science and Technology of Synthetic Metals 152.1 (Sept. 2005), pp. 273–276. ISSN: 0379-6779. DOI: 10.1016/j.synthmet.2005.07.104.
- [30] Xihua Chen et al. “Electronic Structures and Nonlinear Optical Properties of Trinuclear Transition Metal Clusters M-(μ-S)-M’ (M = Mo, W; M’ = Cu, Ag, Au)”. In: *Inorg. Chem.* 42.2 (Jan. 2003), pp. 532–540. ISSN: 0020-1669. DOI: 10.1021/ic025649e.
- [31] Oliver D. Häberlen et al. “Relativistic Density-Functional Studies of Naked and Ligated Gold Clusters”. In: *International Journal of Quantum Chemistry* 52.S28 (1994), pp. 595–610. ISSN: 1097-461X. DOI: 10.1002/qua.560520853.
- [32] M. W. Chase. “NIST-JANAF Thermochemical Tables, Fourth Edition”. In: *J. Phys. Chem. Ref. Data, Monograph 9* (1998), pp. 1–1951.
- [33] Md Abu Bakar et al. “Hydrogen Bonds to Au Atoms in Coordinated Gold Clusters”. In: *Nat Commun* 8.1 (Sept. 2017), p. 576. ISSN: 2041-1723. DOI: 10.1038/s41467-017-00720-3.

- [34] Yukatsu Shichibu et al. “[Au7]3+: A Missing Link in the Four-Electron Gold Cluster Family”. In: *J. Am. Chem. Soc.* 136.37 (Sept. 2014), pp. 12892–12895. ISSN: 0002-7863. DOI: 10.1021/ja508005x.
- [35] Yukatsu Shichibu, Yutaro Kamei, and Katsuaki Konishi. “Unique [Core+two] Structure and Optical Property of a Dodeca-Ligated Undecagold Cluster: Critical Contribution of the Exo Gold Atoms to the Electronic Structure”. In: *Chem. Commun.* 48.61 (July 2012), pp. 7559–7561. ISSN: 1364-548X. DOI: 10.1039/C2CC30251A.
- [36] Kohei Susukida et al. *CCDC 2023935: Experimental Crystal Structure Determination*. DOI: 10.5517/CCDC.CSD.CC25Y27G.
- [37] M. Schulz-Dobrick and M. Jansen. *CCDC 668368: Experimental Crystal Structure Determination*. 2008. DOI: 10.5517/CCQFH8W.
- [38] J. W. A. Van der Velden et al. “Intermediates in the Formation of Gold Clusters. Preparation and x-Ray Analysis of [Au7(PPh3)7]+ and Synthesis and Characterization of [Au8(PPh3)6I]PF6”. In: *Inorg. Chem.* 23.2 (Jan. 1984), pp. 146–151. ISSN: 0020-1669. DOI: 10.1021/ic00170a007.
- [39] Richard E. Marsh. “Crystal Structure of Au7(PPh3)7+: Corrigendum”. In: *Inorg. Chem.* 23.22 (Oct. 1984), pp. 3682–3682. ISSN: 0020-1669. DOI: 10.1021/ic00190a057.
- [40] R. E. Marsh. “Some Thoughts on Choosing the Correct Space Group”. In: *Acta Cryst B* 51.6 (Dec. 1995), pp. 897–907. ISSN: 0108-7681. DOI: 10.1107/S0108768195008901.
- [41] Yi Yang and Paul R. Sharp. “New Gold Clusters [Au8L6](BF4)2 and [(AuL)4](BF4)2 (L = P(Mesityl)3)”. In: *J. Am. Chem. Soc.* 116.15 (July 1994), pp. 6983–6984. ISSN: 0002-7863. DOI: 10.1021/ja00094a082.
- [42] Edgar Zeller, Holger Beruda, and Hubert Schmidbaur. “Tetrahedral Gold Cluster [Au4]2+: Crystal Structure of {[(Tert-Bu)3PAu]4}2+(BF4)2.2CHCl3”. In: *Inorg. Chem.* 32.15 (July 1993), pp. 3203–3204. ISSN: 0020-1669. DOI: 10.1021/ic00067a002.
- [43] Clive E. Briant et al. “Synthesis and Structural Characterisation of Hexakis(Triphenyl Phosphine)Hexagold(2+) Nitrate, [Au6(PPh3)6][NO3]2, and Related Clusters with Edgesharing Bitetrahedral Geometries”. In: *J. Chem. Soc., Dalton Trans.* 3 (Jan. 1986), pp. 687–692. ISSN: 1364-5447. DOI: 10.1039/DT9860000687.
- [44] Pierluigi Bellon, Mario Manassero, and Mirella Sansoni. “An Octahedral Gold Cluster: Crystal and Molecular Structure of Hexakis[Tris-(p-Tolyl)Phosphine]-Octahedro-Hexagold Bis(Tetraphenylborate)”. In: *J. Chem. Soc., Dalton Trans.* 22 (Jan. 1973), pp. 2423–2427. ISSN: 1364-5447. DOI: 10.1039/DT9730002423.
- [45] J. W. A. Van der Velden et al. “Reactions of Cationic Gold Clusters with Lewis Bases. Preparation and x-Ray Structure Investigation of [Au8(PPh3)7](NO3)2.2CH2Cl2 and Au6(PPh3)4[Co(CO)4]2”. In: *Inorg. Chem.* 22.13 (June 1983), pp. 1913–1918. ISSN: 0020-1669. DOI: 10.1021/ic00155a018.

- [46] Jan W. A. Van der Velden et al. “Synthesis and X-ray Crystal Structure Determination of the Cationic Gold Cluster Compound $[\text{Au}_8(\text{PPh}_3)_7](\text{NO}_3)_2$ ”. In: *J. Chem. Soc., Chem. Commun.* 23 (Jan. 1981), pp. 1218–1219. ISSN: 0022-4936. DOI: 10.1039/C39810001218.
- [47] Naoki Kobayashi et al. *CCDC 1001047: Experimental Crystal Structure Determination*. 2014. DOI: 10.5517/CC12LNV5.
- [48] Hui Shen et al. *CCDC 1967410: Experimental Crystal Structure Determination*. DOI: 10.5517/CCDC.CSD.CC2417V9.
- [49] M. Schulz-Dobrick and M. Jansen. *CCDC 615444: Experimental Crystal Structure Determination*. 2007. DOI: 10.5517/CCNNF1R.
- [50] E.A. Malinina et al. *CCDC 687192: Experimental Crystal Structure Determination*. 2008. DOI: 10.5517/CCR22HC.
- [51] Jan M. M. Smits et al. “X-Ray Analysis of Octakis(Tri-p-Tolylphosphine) Enneagoldtris(Hexafluorophosphate), $[\text{Au}_9\{\text{P}(\text{p-MeC}_6\text{H}_4)_3\}_8](\text{PF}_6)_3$: A Redetermination”. In: *Journal of Crystallographic and Spectroscopic Research* 13.5 (Oct. 1983), pp. 365–372. ISSN: 1572-8854. DOI: 10.1007/BF01161299.
- [52] M. Schulz-Dobrick and M. Jansen. *CCDC 690419: Experimental Crystal Structure Determination*. 2009. DOI: 10.5517/CCR5FLX.
- [53] M. Schulz-Dobrick and M. Jansen. *CCDC 690422: Experimental Crystal Structure Determination*. 2009. DOI: 10.5517/CCR5FP0.
- [54] M. Schulz-Dobrick and M. Jansen. *CCDC 615445: Experimental Crystal Structure Determination*. 2007. DOI: 10.5517/CCNNF2S.
- [55] M. Schulz-Dobrick and M. Jansen. *CCDC 690418: Experimental Crystal Structure Determination*. 2009. DOI: 10.5517/CCR5FKW.
- [56] Jia-Qi Wang et al. *CCDC 1895800: Experimental Crystal Structure Determination*. 2019. DOI: 10.5517/CCDC.CSD.CC21MQV8.
- [57] Jia-Qi Wang et al. *CCDC 1895797: Experimental Crystal Structure Determination*. 2019. DOI: 10.5517/CCDC.CSD.CC21MQR5.
- [58] Julia A. Mundy et al. “Liberating a Hidden Antiferroelectric Phase with Interfacial Electrostatic Engineering”. In: *Sci. Adv.* 8.5 (Feb. 2022), eabg5860. ISSN: 2375-2548. DOI: 10.1126/sciadv.abg5860.
- [59] Li Xiao et al. “Structural Study of Gold Clusters”. In: *The Journal of Chemical Physics* 124.11 (Mar. 2006), p. 114309. ISSN: 0021-9606, 1089-7690. DOI: 10.1063/1.2179419.
- [60] Pekka Pyykko. “Relativistic Effects in Structural Chemistry”. In: *Chem. Rev.* 88.3 (May 1988), pp. 563–594. ISSN: 0009-2665. DOI: 10.1021/cr00085a006.
- [61] Henrik Grönbeck and Peter Broqvist. “Comparison of the Bonding in Au 8 and Cu 8 : A Density Functional Theory Study”. In: *Phys. Rev. B* 71.7 (Feb. 2005), p. 073408. ISSN: 1098-0121, 1550-235X. DOI: 10.1103/PhysRevB.71.073408.

- [62] Grant E. Johnson et al. “Cationic Gold Clusters Ligated with Differently Substituted Phosphines: Effect of Substitution on Ligand Reactivity and Binding”. In: *Phys. Chem. Chem. Phys.* 17.22 (2015), pp. 14636–14646. ISSN: 1463-9076, 1463-9084. DOI: 10.1039/C5CP01686J.
- [63] Jinlan Wang, Guanghou Wang, and Jijun Zhao. “Density-Functional Study of Au_n (n = 2 – 20) Clusters: Lowest-energy Structures and Electronic Properties”. In: *Phys. Rev. B* 66.3 (July 2002), p. 035418. ISSN: 0163-1829, 1095-3795. DOI: 10.1103/PhysRevB.66.035418.
- [64] Vlasta Bonačić-Koutecký et al. “Density Functional Study of Structural and Electronic Properties of Bimetallic Silver–Gold Clusters: Comparison with Pure Gold and Silver Clusters”. In: *The Journal of Chemical Physics* 117.7 (Aug. 2002), pp. 3120–3131. ISSN: 0021-9606, 1089-7690. DOI: 10.1063/1.1492800.
- [65] Jin Zhao, Jinlong Yang, and J. G. Hou. “Theoretical Study of Small Two-Dimensional Gold Clusters”. In: *Phys. Rev. B* 67.8 (Feb. 2003), p. 085404. ISSN: 0163-1829, 1095-3795. DOI: 10.1103/PhysRevB.67.085404.
- [66] G. Kresse and J. Furthmüller. “Efficient Iterative Schemes for Ab Initio Total-Energy Calculations Using a Plane-Wave Basis Set”. In: *Phys. Rev. B* 54.16 (Oct. 1996), pp. 11169–11186. DOI: 10.1103/PhysRevB.54.11169.
- [67] G. Kresse and D. Joubert. “From Ultrasoft Pseudopotentials to the Projector Augmented-Wave Method”. In: *Phys. Rev. B* 59.3 (Jan. 1999), pp. 1758–1775. DOI: 10.1103/PhysRevB.59.1758.
- [68] John P. Perdew, Kieron Burke, and Matthias Ernzerhof. “Generalized Gradient Approximation Made Simple”. In: *Phys. Rev. Lett.* 77.18 (Oct. 1996), pp. 3865–3868. DOI: 10.1103/PhysRevLett.77.3865.
- [69] Badri Narayanan et al. “Describing the Diverse Geometries of Gold from Nanoclusters to Bulk—A First-Principles-Based Hybrid Bond-Order Potential”. In: *J. Phys. Chem. C* 120.25 (June 2016), pp. 13787–13800. ISSN: 1932-7447. DOI: 10.1021/acs.jpcc.6b02934.
- [70] A. Hussain et al. “Two Gold Surfaces and a Cluster with Remarkable Reactivity for CO Oxidation, a Density Functional Theory Study”. In: *Top Catal* 54.5 (Apr. 2011), pp. 415–423. ISSN: 1572-9028. DOI: 10.1007/s11244-011-9672-3.
- [71] Stefan Grimme et al. “A Consistent and Accurate Ab Initio Parametrization of Density Functional Dispersion Correction (DFT-D) for the 94 Elements H–Pu”. In: *J. Chem. Phys.* 132.15 (Apr. 2010), p. 154104. ISSN: 0021-9606. DOI: 10.1063/1.3382344.
- [72] Hannu Häkkinen, Michael Moseler, and Uzi Landman. “Bonding in Cu, Ag, and Au Clusters: Relativistic Effects, Trends, and Surprises”. In: *Phys. Rev. Lett.* 89.3 (June 2002), p. 033401. ISSN: 0031-9007, 1079-7114. DOI: 10.1103/PhysRevLett.89.033401.